Effect of Graphene Nanoplatelets Content on the Mechanical and Wear Properties of AZ31 Alloy

Tianhui Lu [1], Mingyang Zhou [2] , Lingbao Ren [3], Lingling Fan [1], Yangyang Guo [1], Xiaoni Qu [1], Hongtao Zhang [1], Xianwen Lu [1] and Gaofeng Quan [1,*]

[1] Key Laboratory of Advanced Technologies of Materials, Ministry of Education, School of Materials Science and Engineering, Southwest Jiaotong University, Chengdu 610031, China; lu13550903862@163.com (T.L.); fanllswjtu@163.com (L.F.); 15108226903@163.com (Y.G.); xiaoniqu@163.com (X.Q.); zht1547986876@126.com (H.Z.); luxianwen1998@163.com (X.L.)

[2] Science and Technology on Reactor System Design Technology Laboratory, Nuclear Power Institute of China, Chengdu 610213, China; 18782951516@163.com

[3] Center for Advancing Materials Performance from the Nanoscale, State Key Laboratory for Mechanical Behavior of Materials, Xi'an Jiaotong University, Xi'an 710049, China; 13281288120@163.com

* Correspondence: quangf@swjtu.edu.cn; Tel.:+86-28-8763-4673

Abstract: Graphene, as a rising-star materials, has attracted interest in fabricating lightweight self-lubricating metal matrix composites with superior mechanical and wear properties. In this work, graphene nanoplatelets (GNPs) reinforced AZ31 alloy composites were fabricated by a powder metallurgy technique and then a hot extrusion. The effects of GNPs content (0.5, 1.0, and 2.0 wt.%) on the microstructures, mechanical properties, and wear performance of the extruded GNPs/AZ31 composites were studied. It was found that the addition of GNPs resulted in a weakened basal plane texture and grain refinement of the AZ31 matrix metal. Less than 1.0 wt.% GNPs in GNPs/AZ31 composites resulted in the enhancement in both Vickers hardness and tensile yield strength with acceptable elongation. The Vickers hardness and tensile yield strength of 1.0GNPs/AZ31 composite increased by 4.9% and 9.5% respectively, compared with the unreinforced AZ31. Moreover, the elongation of the composites was about the same as the AZ31 base alloy. Both the friction coefficient and the wear mass loss continuously decreased with the increasing GNPs content, which exhibited a self-lubricating effect. The relationship of the friction coefficient and wear mass loss with the GNPs content could be modeled in terms of the Holliday model and the exponential decay model, respectively. The worn surface morphology revealed that adhesive wear and abrasive wear simultaneously acted in AZ31 alloy. Nevertheless, abrasive wear became the dominant wear mechanism in the GNPs/AZ31 composites.

Keywords: magnesium matrix composites; graphene nanoplatelets; mechanical properties; wear performance

1. Introduction

Magnesium (Mg) alloys have attracted more and more attentions in the lightweight application of automobiles, electronic equipment and aircrafts because of their low density featuring high specific strength [1,2]. In most circumstances, service requires both high wear resistance and high strength for some assembly parts in martial, automotive, aeronautic and astronautic fields. Metal matrix composites provide a promising approach to improve both the wear resistance and strength, and the suitable reinforcement plays a vital role in achieving the desired performance. According to the mechanism of improving wear resistance, the reinforcement can be divided into hard particles, like SiC, Al_2O_3 and

TiB_2 etc, and self-lubricating materials, such as graphite, carbon nanotubes (CNTs) and graphene nanoplatelets (GNPs) [3]. A lot of previous research [4,5] has indicated that the hard particles improved wear resistance of the composites by increasing the hardness. However, the too low elongation of the hard-particles-containing composites was usually unacceptable. The self-lubricating effect of graphite has been found to be effective to obtain high wear resistance. However, the balance between the wear performance and the mechanical properties does not allow the application of the graphite containing composites [6,7]. For example, Baradeswaran et al. [7] fabricated a 5 wt.% graphite reinforced 7075 composite with superior wear performance, however the strength was too low to be accepted with the counterpart alloys.

GNPs is ideal reinforcement to obtain the appreciable self-lubricating composites with a good combination of wear resistance and mechanical properties, due to the excellent lubricant nature and remarkable mechanical property [8,9]. Many researchers [9–11] focused on exploring the strengthening effect of GNPs on metal matrix. The enhanced overall strength and ductility of Mg matrix composites were achieved by the low content GNPs [10]. Moreover, more and more studies were devoted to research wear behavior in self-lubricating metal matrix composites reinforced by GNPs, and the results indicated the GNPs could reduce the friction coefficient and gave rise to better wear performance [8,12,13]. Kumar et al. [12] revealed that incorporating graphene into Al6061 alloy effectively increased the hardness and suppressed wear loss at proper content. Ghazaly et al. [13] reported the effect of graphene content on the wear properties of graphene reinforced AA2124 alloy composites and found that the 3 wt.% graphene significantly improved the wear resistance of the composites because of self-lubricating of graphene. Nevertheless, there is little research about self-lubricating Mg matrix composites reinforced with carbonous nanomaterials. Arab et al. [14] successfully incorporated GNPs into the AZ31 alloy matrix and found that the composite's friction coefficient decreased by nearly 45% compared to the base alloy. They attributed the superior wear performance to the role of GNPs which not only increased the hardness but also formed a lubricant layer. Wu et al. [15] found that GNPs could simultaneously improve the compressive strength and tribological resistance of AZ31 alloy. In an earlier study [16], we successfully fabricated CNTs reinforced AZ31 composites using a powder metallurgy method, and found that the formation of carbon film could effectively improve the wear performance of the AZ31 alloy. Meanwhile, the strength of AZ31 alloy was significantly improved by adding suitable CNTs. These carbonous nanomaterials stated tremendous potential in simultaneous improving mechanical and wear properties. However, there is little reportage about the mechanical and wear effects of GNPs on self-lubricating Mg matrix composites. Thus, revealing the effects of GNPs content on the mechanical properties and wear performance is beneficial to achieve the excellent combination of the strength and wear performance.
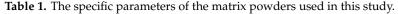
Accordingly, xGNPs/AZ31 (x = 0.5, 1.0, 2.0 wt.%) composites were fabricated by a powder metallurgy method and then a hot extrusion. The effects of GNPs content on the microstructures, mechanical properties and wear performance of AZ31 alloy were investigated. Further, the effects of GNPs on the strengthening mechanism and wear mechanism of the GNPs/AZ31 composites were discussed.

2. Materials and Experimental Procedures

2.1. Materials

The pure Mg, Al, and Zn powders (see Table 1) were used to fabricate Mg–3.0Al–1.0Zn (wt.%) (AZ31) base alloy. These metal powders were supplied by CHINO New Material Technology Co. Ltd. The GNPs (see Figure 1) had about 5–20 nm average thickness, and 10–20 μm flake diameter, purchased from Changzhou Sixth Element Material Technology Co. Ltd.

Table 1. The specific parameters of the matrix powders used in this study.

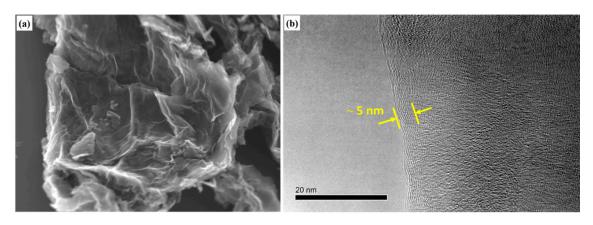| Materials	Mg	Al	Zn
Purity (%)	>99.9	>99.8	>99.8
Particle size (μm)	45	10	10

Figure 1. Characteristics of GNPs: (**a**) TEM image of GNPs; and (**b**) SEM image of GNPs.

2.2. Fabrication of GNPs/AZ31 Composites

The xGNPs/AZ31 (x = 0.5, 1.0, 2.0 wt.%) composites were fabricated by powder metallurgy technique, which were termed as 0.5GNPs/AZ31, 1.0GNPs/AZ31, and 2.0GNPs/AZ31, respectively. First, the GNPs, pure Mg, pure Al, and pure Zn powders were placed in a stainless-steel jar according to the designed proportion, and 0.3 wt.% stearic acid also was adopted to minimize the cold-welding during ball milling. The powders were ball milled at 400 rpm for 2.5 h in which 8 min break intermitting was performed every 20 min milling to prevent overheating. Ar protective atmosphere was input into the jar to minimize the oxidation. The weight ratio of the stainless-steel milling balls to mixture powder was 20:1. The homogeneously milled powders were then uniaxially compacted in a cylindrical steel die under 600 MPa holding for 3 min at ambient temperature (RT). Subsequently, the 60 mm diameter compacted cylinders were sintered at 500 °C for 3 h under Ar gas atmosphere without demold. Finally, these sintered billets were hot pressed at 400 °C under 300 MPa to obtain Φ60 mm × 45 mm compacts. Furthermore, these hot press billets were extruded at 400 °C using an extrusion ratio of 16:1 to obtain Φ15 mm rods. The unreinforced AZ31 alloy rod, served as counterpart alloys, was prepared by the same route line. All the specimens for microstructural characterization and mechanical and wear tests were cut from the middle of these hot extruded rods.

2.3. Characterization

The experimental density was measured using the Archimedean principle, and the theoretical density was estimated by the rule-of-mixture principle. A PANalytical X'Pert Pro X-ray diffraction (Almeo, The Netherland) was performed on the cross sections to character the phase composition in a range of 10°–90° with Cu Kα radiation. The Zeiss A1 optical microscopy (Oberkochen, Germany) and Quanta FEG scanning electron microscope (SEM) (Hillsboro, OR, USA) equipped with an energy dispersive spectroscope (EDS) were employed for the metallography characterization of the microstructure, the fracture morphology, and the wear surface. A 5 (or 15) kV electron beam was used for the SEM observation with a working distance of 10 mm. The observation surface of all microstructure was polished and etched with the picric acid solution (2.1 g picric acid, 5 mL acetic acid, 5 mL distilled water, and 50 mL ethyl alcohol). The grain size distribution was measured and statistical analysis by Matlab program where at least 6 vertices were selected for each grain to form a closed the polygon considered to represent a grain. Moreover, the statistical results were based on at least three OM images.

The Vickers hardness was determined at 1 kgf load, and 15 s dwell time. Seven repeated tests were made on the polished cross-sectional surface of each composition and the hardness values were averaged. The uniaxial tensile tests were conducted on MTS CMT-5105 universal tension machine (Beijing, China). The tensile specimens had 5 mm diameter and 25 mm gauge length paralleled to extrusion direction, and the initial strain rate was 10^{-3} s^{-1}. Three repeat tests were conducted at RT and the testing results were averaged.

The wear performance at RT was studied on the cross sections of extruded samples using a ball on disk testing machine under three loads, namely 5, 10 and 50 N, and sliding distances of 1000 μm. The GCr15 counter ball had 57 HRC, and the dimension of the testing specimen was Φ15 mm × 5 mm.

3. Results and Discussion

3.1. Effect of GNPs on Relative Density and Microstructure

Table 2 shows the density and relative density of the as-extruded AZ31 and the GNPs/AZ31 composites. The theoretical densities of the GNPs/AZ31 composites increased with the increasing GNPs content because the intrinsic density of GNPs (2.25 g/cm^3) was higher than that of AZ31 alloy. The experimental density was slightly different from the theoretical density in all samples. This was because of the existence of inevitable gas in the powder metallurgy process [17]. In addition, the relative density of AZ31 base alloy was 99.63%, which was attributed to the heat densification and severe plastic deformation. However, the porosities of GNPs/AZ31 composites raised with increasing GNPs content. This was because of the poor wettability between GNPs and Mg matrix [9,18]. Moreover, GNPs tended to agglomeration with the increase in content due to its high specific surface area, thus it led to more micro-voids [9,19].

Table 2. Density and relative density of the as-extruded AZ31 and GNPs/AZ31 composites.

Samples	Theoretical Density (g·cm^{-3})	Experimental Density (g·cm^{-3})	Relative Density (%)	Porosity (%)
AZ31	1.7703	1.7637	99.63	0.37
0.5GNPs/AZ31	1.7724	1.7450	98.45	1.55
1.0GNPs/AZ31	1.7744	1.7356	97.81	2.19
2.0GNPs/AZ31	1.7786	1.7150	96.42	3.58

Figure 2 presents the XRD pattern of the unreinforced AZ31 alloy and the GNPs/AZ31 composites. The α-Mg phase was detected in all samples, and the peaks of $Mg_{17}Al_{12}$ and GNPs were not observed in GNPs/AZ31 composites which may be due to low content of the Al and GNPs [20]. The existence of GNPs in composites can be identified by comparing the relative intensity of texture [21,22]. Table 3 shows that relative intensities of the basal plane (I_{basal}/I_{max}) decreased with increasing GNPs content, indicating that GNPs can weaken thfe basal plane texture of AZ31 alloy. However, the I_{basal}/I_{max} in the 1.0GNPs/AZ31 composite and the 2.0GNPs/AZ31 composite were the same which might be ascribed to the aggregation of GNPs, leading to the same effective content of GNPs. It is well-known that the increase in the average basal slip Schmid factor along the tensile direction is beneficial to more easy-activation of the basal slip [23–25]. Thus, the weakening basal texture may improve the ductility by mediating the basal slip Schmid factor.

Figure 3 illustrates the optical micrographs of the AZ31 alloy and the GNPs/AZ31 composites, and Figure 4 shows the corresponding grain size distribution. GNPs refine grain size of the base alloy in the study, and the coarse grains about 13 μm were surrounded by fine recrystallized grains about several microns. However, after adding 2wt.% GNPs, the grain refinement effect was weakened. In addition, the dark area at the grain boundaries increases with increasing weight fraction of GNPs. The EDS mapping analysis of 2.0GNPs/AZ31 composite (see Figure 5) has shown the dark areas in the grain boundaries are abundant in C elements which may correspond to GNPs agglomeration.

The agglomeration of GNPs would not only degrade the grain refinement effect, but also deteriorate the densification and mechanical properties of the GNPs/AZ31 composite.
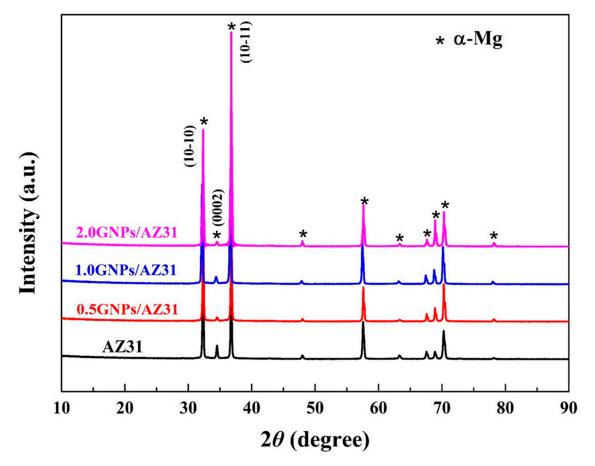

Figure 2. XRD pattern of the unreinforced AZ31 alloy and the GNPs/AZ31 composites.

Table 3. Texture results of AZ31 alloy and the GNPs/AZ31 composites based on XRD.

Samples	Plane		I/Imax
AZ31	{0002}	Basal	0.10
	$\{10\bar{1}0\}$	Prism	1.00
	$\{10\bar{1}1\}$	Pyramidal	0.67
0.5GNPs/AZ31	{0002}	Basal	0.06
	$\{10\bar{1}0\}$	Prism	0.99
	$\{10\bar{1}1\}$	Pyramidal	1.00
1.0GNPs/AZ31	{0002}	Basal	0.02
	$\{10\bar{1}0\}$	Prism	0.54
	$\{10\bar{1}1\}$	Pyramidal	1.00
2.0GNPs/AZ31	{0002}	Basal	0.02
	$\{10\bar{1}0\}$	Prism	0.83
	$\{10\bar{1}1\}$	Pyramidal	1.00

Figure 3. Optical micrographs of the AZ31 and the GNPs/AZ31 composites: (**a**) AZ31, (**b**) 0.5GNPs/AZ31, (**c**) 1.0GNPs/AZ31, and (**d**) 2.0GNPs/AZ31.
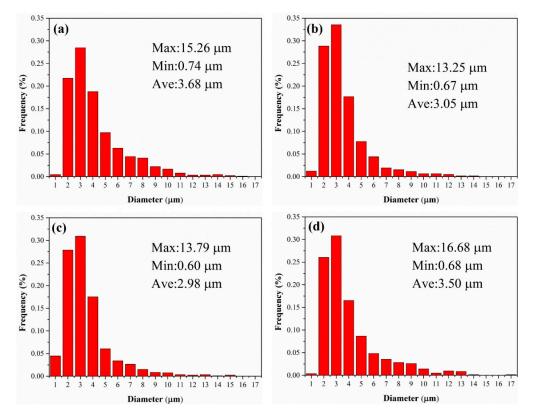

Figure 4. Grain size distribution of the AZ31 and the GNPs/AZ31: (**a**) AZ31, (**b**) 0.5GNPs/AZ31, (**c**) 1.0GNPs/AZ31, and (**d**) 2.0GNPs/AZ31.
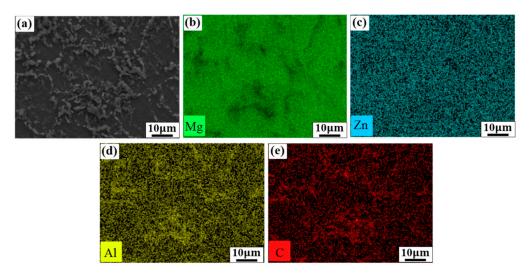
Figure 5. (**a**) SEM images of the 2.0GNPs/AZ31 composites, and (**b–e**) EDS mapping of Mg, Zn, Al and C, respectively.

3.2. Effect of GNPs on Mechanical Properties

Figure 6 shows the mechanical properties of the AZ31 alloy and the GNPs/AZ31 composites, and Table 4 lists the specific value of tensile yield strength (TYS), ultimate tensile strength(UTS), elongation and microhardness. As shown in Figure 6a, the Vickers hardness continuously increased with the increase of GNPs content, and the Vickers hardness of the as-extruded GNPs/AZ31 increased to 87.5 ± 2.2 HV when added 2.0 wt.% GNPs. The GNPs, with high stiffness and hardness [21], contributed higher restraint to the localized deformation than that of the metal matrix resulting in enhanced Vickers hardness [17]. Table 4 shows that the TYS of 0.5GNPs/AZ31, 1.0GNPs/AZ31, and 2.0GNPs/AZ31 were 196 ± 3.2 MPa, 206 ± 4.1 MPa, and 215 ± 5.5 MPa, which increased by 4.2%, 9.6%, and 14.4%, respectively, compared with the unreinforced AZ31(188 ± 5.2 MPa). The GNPs strengthening mechanisms in GNPs/AZ31 composites include: (i) load transfer enhancement, which can be due to the large specific surface of GNPs [26]. A large interfacial contact area between GNPs and Mg matrix is beneficial to load transfer effectively leading to high strengthening efficiency in composites; (ii) thermal mismatch enhancement, which is governed by the increase of dislocation densities owing to the difference in the coefficient of thermal expansion between the GNPs and the Mg matrix. The contribution of dislocation to a boost of the composite strength is evidenced by the greatly increased dislocation density of the composites compared to that of pure metal [27,28]; (iii) Orowan looping enhancement, which can be attributable to the GNPs-dislocation interaction. The complex slip systems can be activated in composites at high stress and the pinned dislocations escaping through the free surfaces because shearing through the hard GNPs layers is extremely difficult [29]; and (iv) fine grain strengthening, which can be attributable to high strength and hard of GNPs. The GNPs effectively suppressed grain growth, even though high energy was input through sintering and extrusion. However, the GNPs/AZ31 composites did not reach the predetermined enhancement effect as described above, e.g., the 2.0GNPs/AZ31 increased its TYS by only 14.4% compared with AZ31 base alloy. Firstly, although the load transfer from the matrix to the GNPs can improve the composite strength, the interface compatibility between Mg matrix and GNPs is weak which negatively impacts the reinforcing effect of GNPs [18]. Moreover, the GNPs agglomeration further degrades the bonding efficiency at the interface. Secondly, as the content of GNPs increases, the raising porosity has a certain weakening effect on improving TYS [30].

In general, the trade-off relationship between the TYS and elongation are prevalent in the micro-size particles reinforced Mg composites [31]. In the present work, the elongation of the composites was almost the same as the matrix and TYS was improved concurrently, when the content of GNPs was lower than 1.0 wt.%. This was because the weakening basal texture provided additional easy-activated

slip systems during tensile along extrusion direction. However, the higher GNPs addition (2.0 wt.%) resulted in a rapid decrement in elongation, which could be due to the more formations of GNPs agglomeration and micro-voids. Figure 7 shows a comparison of the strength and ductility of the GNPs reinforced Mg alloy composites in the present work and previous reports [18,22,26,32–35]. This comparison showed a better combination of the tensile yield strength and elongation in the present study when the content of GNPs was lower than 1.0 wt.%.

Figure 6. Effect of the content of GNPs on: (**a**) microhardness, and (**b**) the tensile properties.

Table 4. Mechanical properties of AZ31 alloy and the GNPs/AZ31 composites.

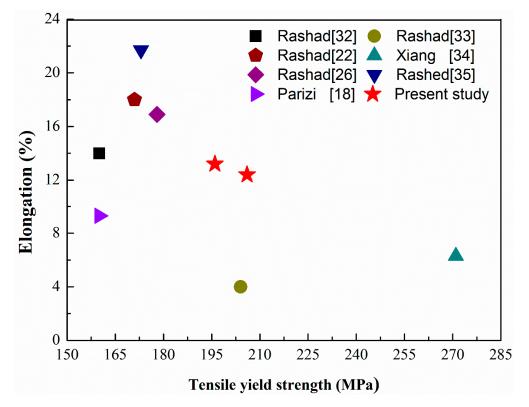| Samples	TYS (MPa)	UTS (MPa)	Elongation (%)	Microhardness (HV)
AZ31	188 ± 5.2	280 ± 2.2	14.4 ± 1.1	81.1 ± 1.1
0.5GNPs/AZ31	196 ± 3.2	282 ± 4.3	13.2 ± 1.3	83.5 ± 1.5
1.0GNPs/AZ31	206 ± 4.1	274 ± 3.8	12.4 ± 1.8	85.1 ± 1.5
2.0GNPs/AZ31	215 ± 5.5	278 ± 2.2	8.9 ± 2.0	87.5 ± 2.2

Figure 7. Comparison of tensile properties of the GNPs reinforced Mg alloy composites with previous studies.

Figure 8 demonstrates tensile fracture morphology of AZ31 alloy and the GNPs/AZ31 composites. Both cleavage steps and dimples remained in all samples exhibiting the brittle and ductile fractures mixed fracture feature. The micro-voids (red arrows) occurred in the 1.0GNPs/composite. Moreover, the number of the micro-voids increased with further increasing the content of GNPs. These micro-voids resulted in the poor elongation.
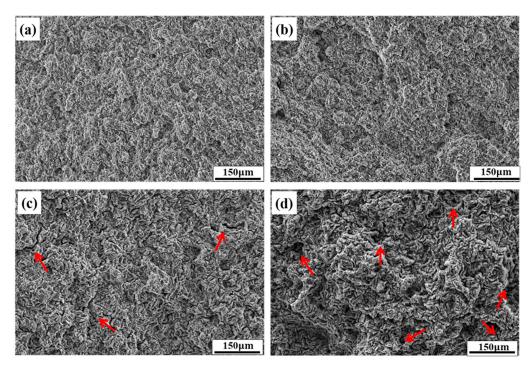

Figure 8. SEM images of the fracture morphology of AZ31 and its composites: (**a**) AZ31, (**b**) 0.5GNPs/AZ31, (**c**) 1.0GNPs/AZ31, and (**d**) 2.0GNPs/AZ31.

3.3. Effect of GNPs on Wear Performance

Variations of the coefficient of friction (COF) with GNPs content are shown in Figure 9. GNPs addition in AZ31 significantly reduced the COF in present study, and the minimum COF was obtained in the 2.0GNPs/AZ31 composite for all range of normal loads ranging between 5–50 N. For example, the COF of AZ31 decreased from 0.50 to 0.42 after adding 2.0 wt.% GNPs at a constant normal load of 5 N, indicating GNPs was responsible for enhancing the wear resistance. Similar property has also been obtained in GNPs reinforced other types of alloy, such as Cu [36] and Al [12]. Both Ghazaly et al. [13] and Xu et al. [37] studied the tribological performance of graphene reinforced metal matrix composites, and found that graphene formed a lubricating tribolayer to reduce the overall COF. Therefore, the reduction of the COF can be attributed to the role of GNPs. Firstly, GNPs can markedly enhance the hardness of the matrix to resist surface plastic deformation. Secondly, GNPs can form a self-lubricating film to reduce tribosurface of two contacting bodies [38]. And as the content of GNPs increases, the self-lubricating films get more continuous and thicker to further reduce the COF of composites [39]. Rajkumar et al. [40] also pointed out that enough self-lubricating film do not exist on the contact zone at low content of nanographite. Further, Figure 9 shows a reduction in the COF as the applied load increased from 5 N to 50 N in same content of GNPs. Increasing applied load can result in increasing in ploughing force which penetrates inside the materials, and hence generate more pull-out of GNPs from the composites, improving the lubrication efficiency of the GNPs film. Moreover, Table 5 shows that the relationships between the content of GNPs (W_{GNPs}) and the COF at various applied load can be described by Holliday model which can predict the COF during the GNPs content between 0.0 to 2.0 wt.% in the study.
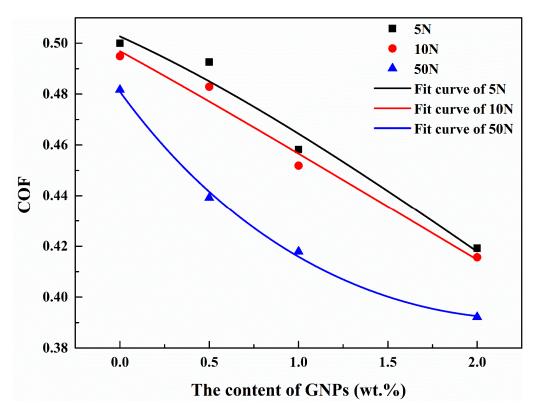
Figure 9. Variation of COF with varying GNPs content.

Table 5. Regression equations of the COF versus WGNPs.

No.	Load(N)	Equations	R-Square
1	5	$y_{5N} = \dfrac{1.0}{1.99 + 0.13w_{GNPs} + 0.04w_{GNPs}^2}$	0.92
2	10	$y_{10N} = \dfrac{1.0}{2.01 + 0.16w_{GNPs} + 0.02w_{GNPs}^2}$	0.95
3	50	$y_{50N} = \dfrac{1.0}{2.08 + 0.42w_{GNPs} - 0.09w_{GNPs}^2}$	0.99

Mass loss is a direct indication of wear resistance of material. Figure 10 shows variations of the wear mass loss with the GNPs contents. The wear mass loss exhibited a decreasing trend as increasing GNPs content under a same applied load. The trend was in agreement with the Archard model in which an increase in hardness of the material led to an enhancement in the wear resistance [41]. Therefore, wear mass loss could be lowest in the case of 2.0GNPs/AZ31 composite. In addition, GNPs acted as a solid lubricant to avoid the matrix and the counter material contact, which resulted in reduction of the wear mass loss [8]. It is proposed that the beneficial role of GNPs on improving the wear resistance. However, the decreasing trend of mass loss is gradually slowing down, which may come from the GNPs agglomeration at high weight fraction of GNPs. Moreover, an increase in the load led to a continuous increase in the wear mass loss with similar GNPs content. It is well-known that the ploughing effect increases as the applied load increases, which results in increasing mass loss. However, the wear mass loss of AZ31 alloy obviously increased, while it was lower in GNPs/AZ31 composites. In addition, based on the distribution of the points in Figure 10, the exponential decay model fitted the curves of the wear mass loss with the content of GNPs, and the fitted results are represented in Table 6.
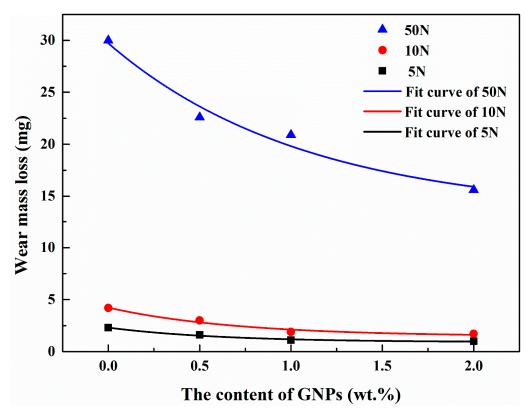
Figure 10. Variations of wear mass loss with varying GNPs content.

Table 6. Regression equations of the mass loss versus WGNPs.

No.	Load(N)	Equations	R-Square
1	50	$y_{50N} = 13.36 + 16.36 \exp^{(-W_{GNPs}/1.08)}$	0.93
2	10	$y_{10N} = 1.46 + 2.78 \exp^{(-W_{GNPs}/0.70)}$	0.93
3	5	$y_{5N} = 0.91 + 1.40 \exp^{(-W_{GNPs}/0.62)}$	0.96

Figure 11 shows the morphologies of the worn surface of AZ31 and its composites. The longitudinal grooves in the sliding direction existed in all samples due to the ploughing effect [42]. The worn surface of GNPs/AZ31 composites were smoother than that of AZ31 alloy. The severe delamination was observed in the AZ31 alloy while there was little delamination in the GNPs/AZ31 composites, and the size of debris became smaller than that of AZ31. This indicates that GNPs are beneficial to improving wear performance and protecting the substrate surface in the wear test. It is evident that worn surface results showed good agreement with existing results of the COF and wear mass loss, as shown in Figures 9 and 10. Worn surface indicated that the dominant wear mechanism of AZ31 alloy were abrasive and adhesive. With the increase of GNPs content, the abrasive became the dominant wear mechanism [15,43]. When GNPs are embedded into AZ31, the wear performance of the composites significantly improves in comparison to unreinforced AZ31.
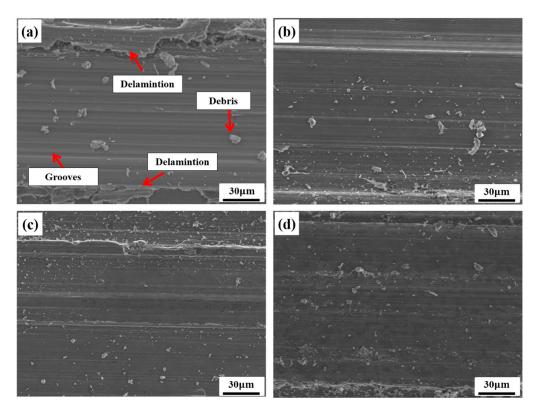
Figure 11. SEM images of the worn surface of AZ31 and its composites: (**a**) AZ31, (**b**) 0.5GNPs/AZ31, (**c**) 1.0GNPs/AZ31, and (**d**) 2.0GNPs/AZ31.

4. Conclusions

In this work, AZ31 alloy composites reinforced with the different content (0.5, 1.0, 2.0 wt.%) of GNPs have been fabricated through the powder metallurgy route and then the hot extrusion. The effects of GNPs on mechanical and wear performances of the composites have been investigated. The main conclusions can be drawn as follows:

(1) The addition of GNPs weakened the basal plane texture of the AZ31 matrix alloy and reduced the grain size of the matrix metal.

(2) Less than 1.0 wt.% GNPs in GNPs/AZ31 composites resulted in the enhancement in both Vickers hardness and tensile yield strength with acceptable elongation. The Vickers hardness and tensile yield strength of 1.0GNPs/AZ31 composite increased by 4.9% and 9.5% respectively. Moreover, the elongation of the composites was about the same as the AZ31 base alloy.

(3) The composites had a lower friction coefficient and less wear mass loss under applied loads than that of unreinforced AZ31 alloy. Moreover, adhesive wear and abrasive wear simultaneously existed in AZ31 alloy, while abrasive wear became the dominant wear mechanism with the increase of GNPs content.

(4) The content of GNPs was varied from 0 wt.% up to 1 wt.%, which resulted in a good combination of wear resistance and mechanical properties.

References

1. Pollock, T. Weight Loss with Magnesium Alloys. *Science* **2010**, *328*, 986–987. [CrossRef] [PubMed]
2. Ren, L.; Fan, L.; Zhou, M.; Guo, Y.; Zhang, Y.; Boehlert, C.; Quan, G. Magnesium application in railway rolling stocks: A new challenge and opportunity for lightweighting. *Int. J. Light. Mater. Manuf.* **2018**, *1*, 81–88. [CrossRef]
3. Zhou, M.; Ren, L.; Fan, L.; Zhang, Y.; Lu, T.; Quan, G.; Gupta, M. Progress in research on hybrid metal matrix composites. *J. Alloy. Compd.* **2020**, *838*, 155274–155313. [CrossRef]
4. Shojaeefard, M.H.; Akbari, M.; Asadi, P.; Khalkhali, A. The effect of reinforcement type on the microstructure, mechanical properties, and wear resistance of A356 matrix composites produced by FSP. *Int. J. Adv. Manuf. Technol.* **2016**, *91*, 1391–1407. [CrossRef]
5. Canakcı, A.; Arslan, F. Abrasive wear behaviour of B4C particle reinforced Al2024 MMCs. *Int. J. Adv. Manuf. Technol.* **2012**, *63*, 785–795. [CrossRef]
6. Omrani, E.; Moghadam, A.D.; Menezes, P.L.; Rohatgi, P.K. Influences of graphite reinforcement on the tribological properties of self-lubricating aluminum matrix composites for green tribology, sustainability, and energy efficiency—A review. *Int. J. Adv. Manuf. Technol.* **2015**, *83*, 325–346. [CrossRef]
7. Baradeswaran, A.; Perumal, A.E. Wear and mechanical characteristics of Al 7075/graphite composites. *Compos. Part B Eng.* **2014**, *56*, 472–476. [CrossRef]
8. Moghadam, A.D.; Omrani, E.; Menezes, P.L.; Rohatgi, P.K. Mechanical and tribological properties of self-lubricating metal matrix nanocomposites reinforced by carbon nanotubes (CNTs) and grapheme—A review. *Compos Part B Eng.* **2015**, *77*, 402–420. [CrossRef]
9. Tjong, S.C. Recent progress in the development and properties of novel metal matrix nanocomposites reinforced with carbon nanotubes and graphene nanosheets. *Mater. Sci. Eng. R Rep.* **2013**, *74*, 281–350. [CrossRef]
10. Xiang, S.; Gupta, M.; Wang, X.; Wang, L.; Hu, X.; Wu, K. Enhanced overall strength and ductility of magnesium matrix composites by low content of graphene nanoplatelets. *Compos. Part A Appl. Sci. Manuf.* **2017**, *100*, 183–193. [CrossRef]
11. Meng, L.; Hu, X.; Wang, X.; Zhang, C.; Shi, H.; Xiang, Y.; Liu, N.; Wu, K. Graphene nanoplatelets reinforced Mg matrix composite with enhanced mechanical properties by structure construction. *Mater. Sci. Eng. A* **2018**, *733*, 414–418. [CrossRef]
12. Kumar, H.G.P.; Xavior, M.A. Fatigue and Wear Behavior of Al6061–Graphene Composites Synthesized by Powder Metallurgy. *Trans. Indian Inst. Met.* **2015**, *69*, 415–419. [CrossRef]
13. Ghazaly, A.; Seif, B.; Salem, H.G. Mechanical and Tribological Properties of AA2124-Graphene Self Lubricating Nanocomposite. In *Light Metals 2013*; Springer: Cham, Switzerland, 2016; pp. 411–415. [CrossRef]
14. Arab, M.; Marashi, S. Effect of graphene nanoplatelets (GNPs) content on improvement of mechanical and tribological properties of AZ31 Mg matrix nanocomposite. *Tribol. Int.* **2019**, *132*, 1–10. [CrossRef]
15. Wu, L.; Wu, R.; Hou, L.; Zhang, J.; Li, M. Microstructure, mechanical properties and wear performance of AZ31 matrix composites reinforced by graphene nanoplatelets(GNPs). *J. Alloy. Compd.* **2018**, *750*, 530–536. [CrossRef]
16. Zhou, M.; Qu, X.; Ren, L.; Fan, L.; Zhang, Y.; Guo, Y.; Quan, G.; Tang, Q.; Liu, B.; Sun, H. The Effects of Carbon Nanotubes on the Mechanical and Wear Properties of AZ31 Alloy. *Materials* **2017**, *10*, 1385. [CrossRef]
17. Li, G.; Xiong, B. Effects of graphene content on microstructures and tensile property of graphene-nanosheets/aluminum composites. *J. Alloy. Compd.* **2017**, *697*, 31–36. [CrossRef]
18. Parizi, M.T.; Ebrahimi, G.; Ezatpour, H. Effect of graphene nanoplatelets content on the microstructural and mechanical properties of AZ80 magnesium alloy. *Mater. Sci. Eng. A* **2018**, *742*, 373–389. [CrossRef]
19. Liu, J.; Yan, H.; Jiang, K. Mechanical properties of graphene platelet-reinforced alumina ceramic composites. *Ceram. Int.* **2013**, *39*, 6215–6221. [CrossRef]
20. Rashad, M.; Pan, F.; Lin, D.; Asif, M. High temperature mechanical behavior of AZ61 magnesium alloy reinforced with graphene nanoplatelets. *Mater. Des.* **2016**, *89*, 1242–1250. [CrossRef]
21. Du, X.; Du, W.; Wang, Z.; Liu, K.; Li, S. Ultra-high strengthening efficiency of graphene nanoplatelets reinforced magnesium matrix composites. *Mater. Sci. Eng. A* **2018**, *711*, 633–642. [CrossRef]
22. Rashad, M.; Pan, F.; Asif, M. Exploring mechanical behavior of Mg–6Zn alloy reinforced with graphene nanoplatelets. *Mater. Sci. Eng. A* **2016**, *649*, 263–269. [CrossRef]

23. Tekumalla, S.; Bibhanshu, N.; Suwas, S.; Gupta, M. Superior ductility in magnesium alloy-based nanocomposites: The crucial role of texture induced by nanoparticles. *J. Mater. Sci.* **2019**, *54*, 8711–8718. [CrossRef]

24. Guo, L.; Chen, Z.; Gao, L. Effects of grain size, texture and twinning on mechanical properties and work-hardening behavior of AZ31 magnesium alloys. *Mater. Sci. Eng. A* **2011**, *528*, 8537–8545. [CrossRef]

25. Huang, X.; Suzuki, K.; Watazu, A.; Shigematsu, I.; Saito, N. Mechanical properties of Mg–Al–Zn alloy with a tilted basal texture obtained by differential speed rolling. *Mater. Sci. Eng. A* **2008**, *488*, 214–220. [CrossRef]

26. Rashad, M.; Pan, F.; Hu, H.; Asif, M.; Hussain, S.; She, J. Enhanced tensile properties of magnesium composites reinforced with graphene nanoplatelets. *Mater. Sci. Eng. A* **2015**, *630*, 36–44. [CrossRef]

27. Feng, S.; Guo, Q.; Li, Z.; Fan, G.; Li, Z.; Xiong, D.-B.; Su, Y.; Tan, Z.; Zhang, J.; Zhang, D. Strengthening and toughening mechanisms in graphene-Al nanolaminated composite micro-pillars. *Acta Mater.* **2017**, *125*, 98–108. [CrossRef]

28. Yang, M.; Liu, Y.; Fan, T.; Zhang, D. Metal-graphene interfaces in epitaxial and bulk systems: A review. *Prog. Mater. Sci.* **2020**, *110*, 100652. [CrossRef]

29. Kim, Y.; Lee, J.; Yeom, M.S.; Shin, J.W.; Kim, H.; Cui, Y.; Kysar, J.W.; Hone, J.; Jung, Y.; Jeon, S.; et al. Strengthening effect of single-atomic-layer graphene in metal-graphene nanolayered composites. *Nat. Commun.* **2013**, *4*, 2114. [CrossRef]

30. Hong, S.H.; Chung, K.H. Effects of vacuum hot pressing parameters on the tensile properties and microstructures of SiC-2124 Al composites. *Mater. Sci. Eng. A* **1995**, *194*, 165–170. [CrossRef]

31. Abdollahi, A.; Alizadeh, A.; Baharvandi, H.R. Comparative studies on the microstructure and mechanical properties of bimodal and trimodal Al2024 based composites. *Mater. Sci. Eng. A* **2014**, *608*, 139–148. [CrossRef]

32. Rashad, M.; Pan, F.; Tang, A.; Lu, Y.; Asif, M.; Hussain, S.; She, J.; Gou, J.; Mao, J. Effect of graphene nanoplatelets (GNPs) addition on strength and ductility of magnesium-titanium alloys. *J. Magnes. Alloy.* **2013**, *1*, 242–248. [CrossRef]

33. Rashad, M.; Pan, F.S.; Tang, A.T.; Asif, M.; Aamir, M. Synergetic effect of graphene nanoplatelets (GNPs) and multi-walled carbon nanotube (MW-CNTs) on mechanical properties of pure magnesium. *J. Alloy. Compd.* **2014**, *603*, 111–118. [CrossRef]

34. Xiang, S.; Wang, X.; Gupta, M.; Wu, K.; Hu, X.; Zheng, M. Graphene nanoplatelets induced heterogeneous bimodal structural magnesium matrix composites with enhanced mechanical properties. *Sci. Rep.* **2016**, *6*, 38824. [CrossRef]

35. Rashad, M.; Pan, F.; Zhang, J.; Asif, M. Use of high energy ball milling to study the role of graphene nanoplatelets and carbon nanotubes reinforced magnesium alloy. *J. Alloy. Compd.* **2015**, *646*, 223–232. [CrossRef]

36. Zhang, Y.; Li, Y.; Song, M.H.; Zhang, X.C. Effect of Graphene Content on Microstructure and Properties of Gr/Cu Composites. *Mater. Sci. Forum* **2020**, *993*, 723–729. [CrossRef]

37. Xu, Z.; Shi, X.; Zhai, W.; Yao, J.; Song, S.; Zhang, Q. Preparation and tribological properties of TiAl matrix composites reinforced by multilayer graphene. *Carbon* **2014**, *67*, 168–177. [CrossRef]

38. Berman, D.; Erdemir, A.; Sumant, A.V. Few layer graphene to reduce wear and friction on sliding steel surfaces. *Carbon* **2013**, *54*, 454–459. [CrossRef]

39. Hidalgo-Manrique, P.; Lei, X.; Xu, R.; Zhou, M.; Kinloch, I.A.; Young, R.J. Copper/graphene composites: A review. *J. Mater. Sci.* **2019**, *54*, 12236–12289. [CrossRef]

40. Rajkumar, K.; Aravindan, S. Tribological behavior of microwave processed copper-nanographite composites. *Tribol. Int.* **2013**, *57*, 282–296. [CrossRef]

41. Archard, J.F. Contact and Rubbing of Flat Surfaces. *J. Appl. Phys.* **1953**, *24*, 981. [CrossRef]

42. Li, J.; Xiong, D. Tribological behavior of graphite-containing nickel-based composite as function of temperature, load and counterface. *Wear* **2009**, *266*, 360–367. [CrossRef]

43. Garcia-Rodriguea, S.; Torres, B.; Maroto, A.; Lopez, J.Z.; Otero, E.; Rama, J. Dry sliding wear behavior of globular AZ91 magnesium alloy and AZ91/SiCp composites. *Wear* **2017**, *390*, 1–10. [CrossRef]